Three-Dimensional Metallic Boron Nitride

Shunhong Zhang,[†] Qian Wang,*[,†,‡] Yoshiyuki Kawazoe,[§] and Puru Jena[‡]

[†]Center for Applied Physics and Technology, College of Engineering, Peking University, Beijing 100871, China
[‡]Department of Physics, Virginia Commonwealth University, Richmond, Virginia 23284, United States
[§]Institute for Material Research, Tohoku University, Sendai, 980-8577, Japan

S Supporting Information

ABSTRACT: Boron nitride (BN) and carbon are chemical analogues of each other and share similar structures such as one-dimensional nanotubes, two-dimensional nanosheets characterized by sp^2 bonding, and three-dimensional diamond structures characterized by sp^3 bonding. However, unlike carbon which can be metallic in one, two, and three dimensions, BN is an insulator, irrespective of its structure and dimensionality. On the basis of state-of-the-art theoretical calculations, we propose a tetragonal phase of BN which is both dynamically *stable* and *metallic*. Analysis of its band structure, density of states, and electron localization function confirms the origin of the metallic behavior to be due to the delocalized B 2p electrons. The metallicity exhibited in the studied three-dimensional BN structures can lead to materials beyond conventional ceramics as well as to materials with potential for applications in electronic devices.
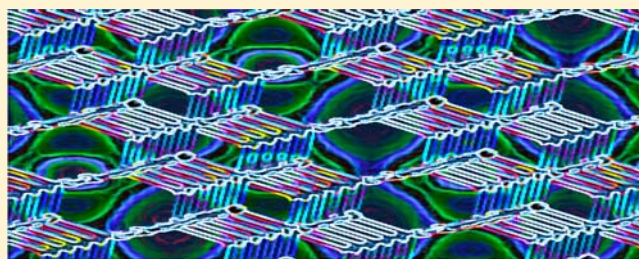
1. INTRODUCTION

Boron and nitrogen, the left and right neighbors of carbon in the periodic table, form an interesting family of binary boron nitride (BN) compounds similar to those of carbon materials but display different mechanical,[1] thermal,[2] optical,[3−5] and catalytic[6] properties. Due to its exceptional thermal and chemical stability compared to carbon-based materials, BN is widely used as a high-temperature ceramic material which can withstand extremely harsh environment. Especially, because of the difference in electronegativity, B and N form strongly polarized covalent bonds and BN is an insulator. Although elementary boron[7] and nitrogen[8] appear to be metallic under high pressure, BN remains an insulator even when severely compressed.[5,9] All currently identified three-dimensional (3D) BN phases are insulating[3,4] including cubic-BN (c-BN), wurtzite BN (w-BN), layered hexagonal BN (h-BN), and rhombic BN (r-BN). No exception to this behavior is found even in the recently predicted new BN polymorphs.[9−14] In two dimensions (2D), monolayer hexagonal BN, known as white graphene, was also found to be an insulator with a wide band gap of around 6.0 eV.[15] Other 2D BN allotropes have been widely studied and found to be semiconducting[16] with wide band gaps. In one-dimensional (1D) systems, BN nanotubes, irrespective of their chirality and radius,[17−19] are insulators, and BN nanoribbons[20,21] are also semiconducting, irrespective of their shape and width. This is in contrast to carbon where nanotubes and graphene nanoribbons can be metallic or semiconducting depending on their chirality and morphology.

Engineering of electronic structure of materials as a way to tailor their electronic properties is a topic of great general interest in science and technology. For instance, extensive

attempts have been made to open the bandgap in gapless graphene[22] and tune semiconducting silicon or germanium from indirect-bandgap to direct-bandgap.[23−25] In the case of BN, practical application in electronic devices is hindered because of its wide band gap. This has stimulated recent research in reducing or even closing the band gap. For example, H-terminated c-BN *thin film* was found to become metallic when its thickness exceeds a critical threshold of 0.69 nm.[26] The band gap closure in BN nanoribbons can also be achieved by introducing foreign atoms[27,28] or applying electric field.[21] However, in many practical applications, 3D structures are preferable over functionalized thin films and edge-decorated nanoribbons. Because metallic 3D BN would be a promising candidate for application in electronic devices, the question arises: is it possible to design and synthesize a new 3D BN structure that can display intrinsic metallicity without introduction of any foreign atoms or application of an external electric field? A comprehensive study is presented here to demonstrate such a possibility.

2. COMPUTATIONAL DETAILS

Determination of Geometry and Electronic Properties. Our calculations are based on density functional theory (DFT) and are performed using the Vienna Ab initio Simulation Package (VASP)[29] with Projector Augmented Wave (PAW) potential.[30] Plane waves with kinetic energy cutoff of 500 eV are used to expand the wave function of valence electrons ($2s^2 2p^3$ for B and $2s^2 2p^5$ for N). When investigating the structural properties, we use the revised Perdew−Burke−Ernzerhof functional for solid (PBEsol)[31,32] within generalized

gradient approximation (GGA) to treat the exchange-correlation interaction between electrons. To ensure an accurate determination of electronic properties, calculations are repeated using the hybrid Heyd−Scuseria−Ernzerhof functional (HSE06).[33,34] Partial occupancy of valence electrons is described using a Gaussian smearing scheme with a width of 0.005 eV. Full geometry optimizations are carried out by using the convergence thresholds of 10^{-4} eV, 10^{-3} eV/Å, and $2\pi \times 0.02$ Å^{-1} for total energy, ionic force component, and k point spacing (Monkhorst−Pack sampling scheme[35]), respectively.

Phonon Properties. Lattice vibrational properties are calculated using the density functional perturbation theory (DFPT).[36] Before calculation of the phonons, the structures are reoptimized using a higher convergence criteria, namely, 10^{-8} eV for total energy and 10^{-6} eV/Å for Hellmann−Feynman Force, respectively. The dynamical matrix is then calculated by VASP 5.2, based on which force constants are calculated using Phonopy code,[37] and phonon band dispersions and frequency DOS are obtained by solving the dynamical equations.

Bader Charge Analysis. Most charge analysis methods such as Mulliken population analysis are based on electron wave functions and thus sensitive to the type and cutoff of basis sets. Bader analysis,[38] on the other hand, makes use of what are called zero flux surfaces to divide atoms, and the analysis is merely dependent on charge density distribution. The charge enclosed within the Bader volume is a good approximation to the total electronic charge of an atom. In our work, Bader charge analysis is performed using the code developed by Henkelman's group.[39−41]

3. RESULTS

Atomic Configuration. The inspiration to search for a new allotrope of BN that is metallic came from the analogy between BN and C. For all-sp^3 bonded structures, both carbon and BN are insulating. However, in the presence of sp^2 hybridization mode, carbon is known to be metallic or semimetallic as in nanotubes (with certain chirality), graphite, and graphene. However, unlike graphene, in the all-sp^2 bonded h-BN sheet, the electronegativity difference between B and N breaks the symmetry of the bipartite honeycomb lattice and leads to the a wide bandgap.[42] Hence, we considered building a sp^2-sp^3 hybrid BN system which can take advantage of boron's electron-deficient feature to create multicenter bonds. In a 3D BN formed with interlocking hexagons, sp^2 and sp^3 configurations can coexist, and metallicity could arise provided electron delocalization can be achieved.

The new 3D BN structure we designed has a *tetragonal* primitive cell (space group $P\bar{4}m2$, no. 115) containing *three* formula units, as shown in Figure 1. We therefore term it as T-B$_3$N$_3$. The optimized lattice parameters are $a = b = 2.64$ Å, and $c = 6.11$ Å. There are four chemically nonequivalent atoms in the primitive cell, labeled as B1, N1, B2, and N2 in Figure 1. Their atomic Wyckoff positions are given in Table 1. The B1 (N1) atom adopts distorted sp^3 hybridization and binds to four N2 (B2) atoms with a bond length of 1.57 Å which is comparable to that in the c-BN and w-BN. The B2 (N2) atom is sp^2-hybridized and each B2 (N2) binds to two N1 (B1) atoms and one N2 (B2) atom. The bond length between N2 and B2 atoms is 1.35 Å, showing unusual double bond character[43,44] which may induce some novel properties in this new polymorph.

Dynamic Stability. We first calculate the phonon dispersion and frequency density of states (DOS) to ensure the dynamical stability of the T-B$_3$N$_3$ structure. The calculated results are plotted in Figure 1d. The absence of soft modes within the entire Brillouin Zone clearly indicates that this configuration corresponds to a minimum in the potential energy surface (PES). A significant phonon gap is observed in
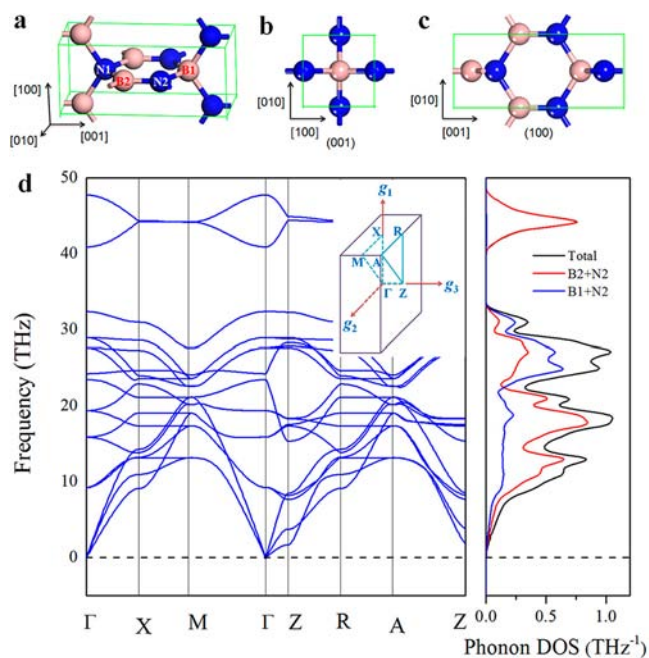

Figure 1. (a) Perspective view, (b) view from the [001] direction, (c) view from the [100] direction, and (d) phonon dispersion and frequency DOS of the T-B$_3$N$_3$ structure. The high symmetry q point path in the Brillouin Zone is chosen as: Γ (0, 0, 0) → X (1/2, 0, 0) → M (1/2, 1/2, 0) → Γ (0, 0, 0) → Z (0, 0, 1/2) → R (1/2, 0, 1/2) →A (1/2, 1/2, 1/2) → Z (0, 0, 1/2) (see the insert).

Table 1. Atomic Positions, Bader Charge and Volume, and Bond Length of the T-B$_3$N$_3$ Structure

atom	Wyckoff position	Bader charge, e	Bader volume (Å^3)	bond length (Å)
B1	1c (0.5, 0.5, 0.5)	0.81	1.70	$d_{B1-N2} = 1.57$
N1	1b (0.5, 0.5, 0.0)	7.23	12.00	$d_{N1-B2} = 1.57$
B2	2g (0.0, 0.5, 0.8602)	0.94	2.39	$d_{B2-N2} = 1.35$
N2	2g (0.0, 0.5, 0.6378)	7.03	12.04	$d_{N2-B2} = 1.35$

the band dispersion, separating the vibrational modes into the low frequency (0−32.4 THz) and the high frequency (40.5−48 THz) regions. The phonon DOS shows that the high frequency modes are entirely contributed by the B2 and N2 atoms, and the partial DOS of (B2 + N2) and total DOS overlap in the high frequency region. Detailed analysis indicates that these modes correspond to vibrations of the double bond formed between the B2 and N2 atoms.

Energetic Stability. Total energy calculations are performed to investigate the thermodynamic stability. The calculated total energy−volume curve for the T-B$_3$N$_3$ is plotted in Figure 2 and compared with some other BN allotropes. From the energetic point of view, the T-B$_3$N$_3$ is found to be metastable as compared to the well-known c-BN and w-BN but has a cohesive energy larger than that of the previously reported rocksalt[5,9] and NiAs-type[9] structures. Due to its nanoporosity, T-B$_3$N$_3$ has lower density at equilibrium than that of the high pressure phases (bct-BN,[9,10] Z-BN,[11,13] P-BN,[14] rocksalt,[5,9] and NiAs-type[9] BN). For comparison, additional calculations were also performed for some BN nanostructures including small BN nanotubes[19] (BNNTs) and BN cages.[45,46] We found that the T-B$_3$N$_3$ is energetically more stable than (3, 0) BNNT, (4, 0)
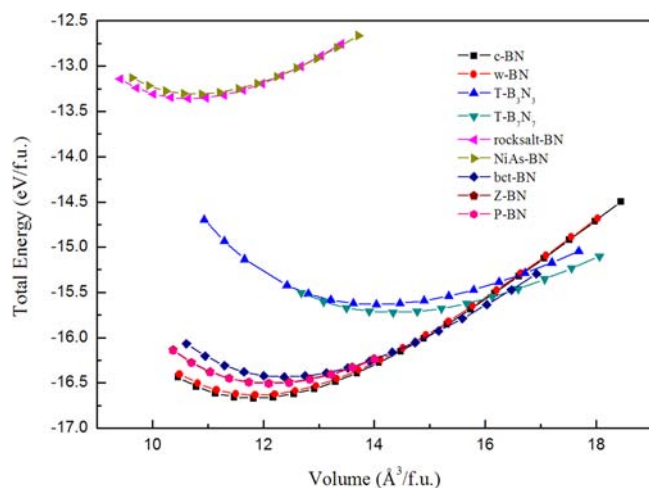
Figure 2. Volume dependence of total energy for some crystalline BN allotropes.

BNNT, and $B_{12}N_{12}$ and $B_{24}N_{24}$ cages, respectively (see Table 2).

Table 2. Cohesive Energies (in eV/f.u.) of Some Nanostructured BN Allotropes Relative to the T-B_3N_3 and T-B_7N_7 Phases

structures	symmetry	relative energy
T-B_3N_3	$P\bar{4}m2$	0.00
T-B_7N_7	$P\bar{4}m2$	−0.09
$B_{12}N_{12}$ cage	T_h	0.64
$B_{24}N_{24}$ cage	S_8	0.26
(3, 0) BNNT	$Pmc2_1$	0.94
(4, 0) BNNT	$P4cc$	0.19

Electronic Properties. The electronic properties of T-B_3N_3 structure is studied by computing the electronic band structure. The results are given in Figure 3a. We see that a partially occupied band (the 13th band from the bottom) crosses the Fermi level in the vicinity of M point in the Brillouin Zone, suggesting that the T-B_3N_3 is metallic. Because standard DFT calculations are well-known to underestimate the band gap, we
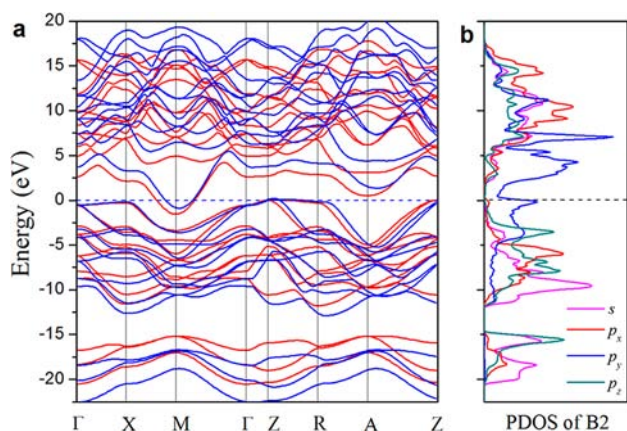

Figure 3. Electronic structure of the T-B_3N_3. (a) Band structure (red: GGA/PBE; blue: HSE06) and (b) projected DOS for the B2 atom in the unit cell (GGA/PBE). The Fermi level is shifted to 0.0 eV. The electronic DOS is in arbitrary units.

repeated the band structure calculations using the screened hybrid functional HSE06[33,34] which has been demonstrated to be more accurate in describing the exchange-correlation energy of electrons in solids. The results are plotted in Figure 3. The partially occupied band-crossing feature at the Fermi level still remains (see Figure 3a), thus confirming the metallicity of T-B_3N_3.

To explore the origin of metallicity, we calculated the DOS projected onto the atomic orbitals of the four nonequivalent atoms in the primitive cell. We note that the electronic states near the Fermi level are mainly contributed by the p_y orbitals of B2, as shown in Figure 3b; the contribution from N2 is small and that from B1 and N1 is negligible. Bader charge analysis (see Table 1) suggests that the B2 atoms have less charge transferred to the neighboring N atoms and have atomic volume (Bader volume) larger than that of the B1 atoms, indicating that electrons in the B2 atoms are more delocalized. To further visualize the partially occupied conduction band in real space, we calculated the band decomposed charge densities. These are plotted in Figure 4a and 4b, showing that the charge
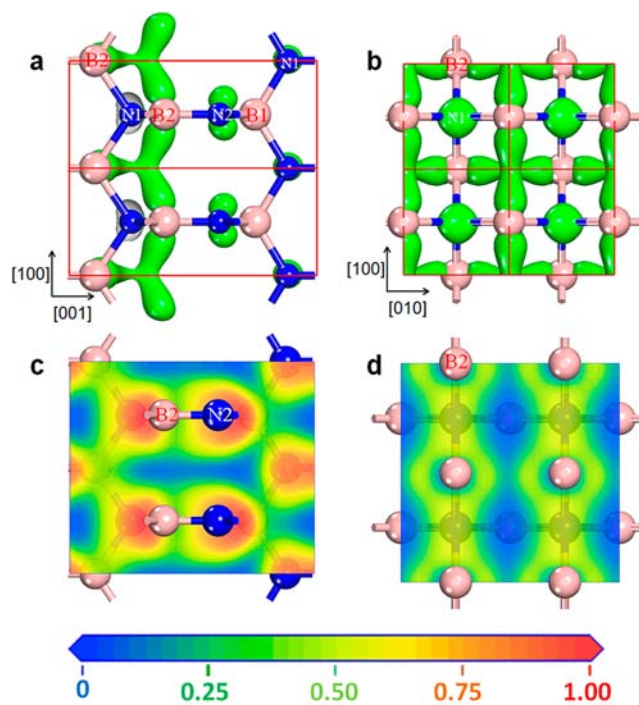

Figure 4. Band decomposed charge density distribution (the 13th band) and slices of electron localization function (ELF) of the T-B_3N_3. Panels a and c are viewed from the [010] direction, and panels b and d from the [00$\bar{1}$] direction. The isovalue for charge density is 0.15 e/Å^3, and the reference bar for ELF value is provided at the bottom.

density of the partially occupied band is mainly contributed by B2 atoms with small contribution from N2 atoms. This is consistent with our observation from the PDOS. It is interesting to note that the charge densities around N1 and B1 are localized, while the charges in the region of the four nearest B2 atoms are delocalized and form a pyramid-like distribution. A conducting network parallel to the (001) crystal surface is thus formed by the two layers of B2 atoms connected by these delocalized electrons. Therefore, it is reasonable to assume that the metallicity of T-B_3N_3 is derived from these delocalized states. The electron localization function (ELF) provides a good description of electron delocalization in

molecules[47] and solids[48] and is a useful tool for chemical bond classification.[49] The ELF refers to the jellium-like homogeneous electron gas and renormalizes the value to between 0.00 and 1.00. The values of 1.00 and 0.50 correspond to fully localized and fully delocalized electrons, respectively, while the value 0.00 refers to very low charge density. We calculated the ELF of T-B_3N_3 to identify its delocalization character. Slices parallel to the (010) and (00$\bar{1}$) crystal faces crossing the B2 atoms are plotted in Figure 4c and 4d, respectively. With the ELF value close to 0.50 resembling that in bulk Al and Al-based clusters,[50] delocalization in the regions near the B2 atoms is evident. This further confirms that the presence of unusual metallicity of T-B_3N_3 is intimately associated with the delocalized states originating from the peculiar atomic configuration.

An Extension of the Metallic Phase. Having elucidated the origin of metallicity in the T-B_3N_3, we extended this structure by increasing the number of B2 and N2 atoms in the unit cell to see if metallicity can be enhanced. This leads to the structure shown in Figure 5a and 5b. We term it as T-B_7N_7, as
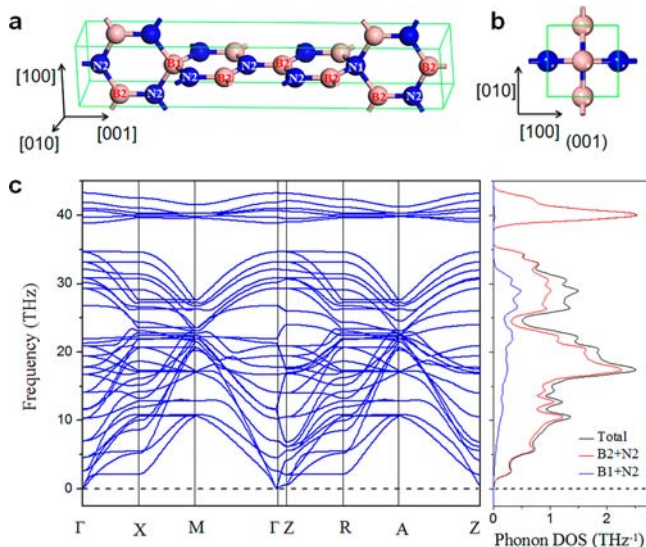

Figure 5. (a) Perspective view, (b) view from the [001] direction, and (c) phonon dispersion and vibrational DOS of the T-B_7N_7 structure.

there are *seven* BN formula units in the primitive cell. Phonon spectra confirm that T-B_7N_7 is also dynamically stable without any imaginary frequency (see Figure 5c). The total energy calculation shows that it has a slightly larger cohesive energy as compared to the T-B_3N_3 structure (see Figure 2 and Table 2). A parallel study on the electronic structure reveals that the T-B_7N_7 is metallic as expected (see the band structure in Figure 6a). The ELF analysis shown in Figure 6b confirms that the delocalized charges are also from B2 sites. A systematic study of the stability and metallicity of T-B_xN_x (x = 11, 15, and 19) has been carried out further. The calculated results are plotted in Figure 7. Similarly, the conducting networks formed by the delocalized electrons in the planes parallel to the (001) face are also observed for all the studied systems with sp^2-sp^3-hybridized BN allotropes. From the calculated total energy, we see that increasing the ratio of B2 and N2 atoms not only enhances the metallicity but also improves the thermodynamic stability, as is shown in Figure 7. This in essence implies a paradigm shift for constructing a metallic BN by "fusing" the AA stacked multilayer h-BN alternatively. This is distinct from the
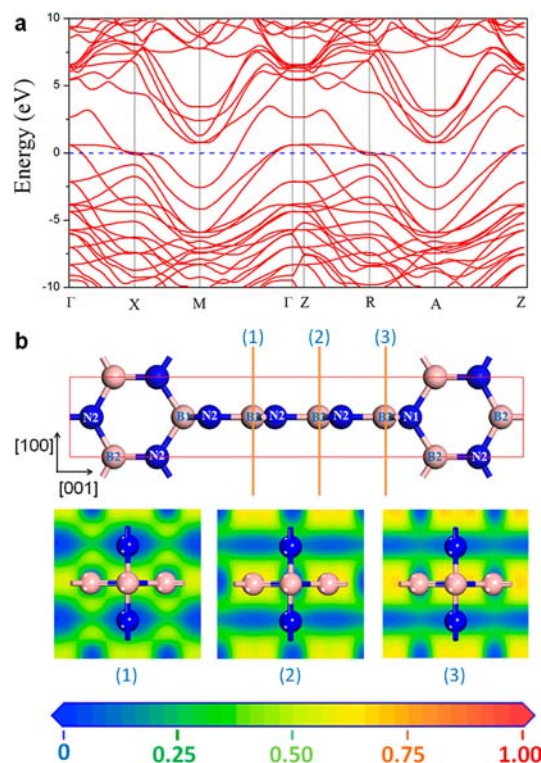

Figure 6. Electronic structure of the T-B_7N_7. (a) Electronic band structure of the T-B_7N_7 using HSE06 functional. The Fermi level is shifted to 0.00 eV. (b) Selected slices 1, 2, and 3 for plotting the ELF. The lower panel with the color map shows the isodensity values.
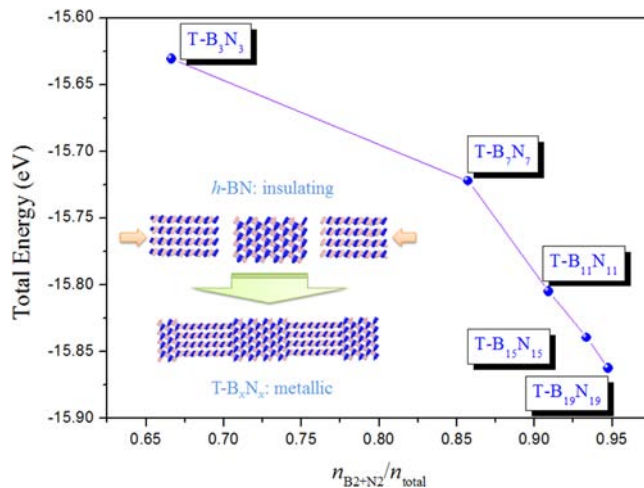

Figure 7. Variation of total energy per BN unit of the metallic T-B_xN_x ($x = 4n - 1$, n = 1, 2, 3, 4, and 5) allotropes with respect to the proportion of B2 and N2 atoms.

conventional compression of h-BN that leads to all sp^3 hybridization and an insulating state.[9−11,13,14] The present "fused" configurations exhibit sp^2-sp^3 hybrid characteristics, where the B1 and N1 atoms with sp^3 bonding anchor the h-BN layers with an interlayer distance of 2.64 Å. This separation is much smaller than that in ordinary layered h-BN structures (3.33 Å[14]). The reduced distance enhances the interlayer interactions, leading to the electron delocalization on the B2 sites with sp^2 configurations and hence resulting in metallicity.

4. DISCUSSION

To better understand the metallicity displayed in the studied 3D BN structures, it is worth recalling the following facts. (1) Boron is a versatile element which can form multielectron-multicenter bonds due to its electron-deficient character.[51] For example, in the well-known superconducting magnesium diboride (MgB_2), B atoms form graphitic layers with Mg intercalated between them. Here the 2p states of B form a delocalized π network responsible for the metallicity of MgB_2, and the strong coupling with the in-plane vibrational modes of B atoms leads to high-T_c superconductivity.[52,53] Therefore, similar to the situation in MgB_2, the metallicity exhibited in T-B_3N_3 is understandable. (2) The electron delocalization feature in T-B_3N_3 is also reminiscent of the well-known BN system, namely, the cyclic borazine ($B_3N_3H_6$). As an inorganic isoelectronic analogue of benzene, the cyclic borazine resembles benzene in structure as well as in some properties. For instance, many studies have found that in both benzene and borazine the π electrons are delocalized overall.[54,55] Although aromaticity in borazine is only half of that of benzene, the unusual parallel behavior between benzene and its BN analogue, borazine, in electron delocalization implies the possibility to achieve metallicity in BN materials. (3) During the revision process, we came to know of a tetragonal carbon allotrope known as "glitter",[56−58] which can be viewed as a chemical analogue of T-B_3N_3. However, the metallicity of "glitter", according to Bucknum et al.,[56−58] is due to its special "spiroconjugation" geometry and the resultant overlap of the dispersive π and π* band near the Fermi level, while the metallicity of T-B_3N_3 is mainly due to the delocalized electrons at B sites. (4) Recent experimental and theoretical advances have demonstrated that some elements would undergo intriguing insulator−metal (like hydrogen[59] and boron[7]) or metal−insulator (like lithium[60−62] and sodium[63]) transitions when the atomic configurations are changed under compression.[64] Here for the first time we show that the well-known insulating BN can become metallic when its atomic configuration is changed. Our finding provides new insights into the understanding of BN materials.

To aid experimentalists in the synthesis of this new phase of BN, we stress that the building blocks of the tetragonal phase of BN are interlocked BN hexagons. This can be achieved by using borazine ($B_3N_3H_6$) as a precursor. Note that borazine is the chemical analogue of benzene (C_6H_6) which has already been used in the synthesis of hexagonal carbon structures such as nanotubes and graphene. Similarly, borazine has been recently used in the synthesis of BN nanotubes and BN sheets.[65,66] The procedure for forming interlocking molecular structures has also been recently discussed by Ayme et al.[67]

5. CONCLUSIONS

In summary, a comprehensive first-principles DFT study of possible metallicity in 3D BN is performed. We have shown that the 3D BN structures composed of interlocking BN hexagons are *metallic* and dynamically *stable*. These newly designed 3D BN structures (T-B_xN_x, $x = 4n − 1$, $n = 1, 2, 3...$) are hybrid systems with *one* B and *one* N atom in sp^3 hybridization and ($4n − 2$) sp^2-bonded B and N atoms respectively per unit cell. The sp^3 bonded B (N) atom binds to its surrounding four sp^2 bonded N (B) atoms forming the 3D backbone and is responsible for stability. The sp^2 bonded B atoms, on the other hand, play the key role in rendering the conducting network and metallicity. This special geometrical feature results in a unique property: unlike previously reported functionalized c-BN thin film whose metallicity stems from strong inbuilt polarization, the metallicity in 3D T-B_xN_x is intrinsic and comes from the delocalized electrons distributed around the B2 sites. The metallicity exhibited in the studied structures opens new door for BN materials with potential applications in electron transport, metal-free catalysis, and electronic devices. We hope that the present theoretical prediction will stimulate experimental interest.

■ ASSOCIATED CONTENT

Ⓢ Supporting Information

Total energies (in Hartrees) and the atomic coordinates of the optimized BN structures studied in this work. This material is available free of charge via the Internet at http://pubs.acs.org.

■ AUTHOR INFORMATION

Corresponding Author

qianwang2@pku.edu.cn

Notes

The authors declare no competing financial interests.

■ ACKNOWLEDGMENTS

■ REFERENCES

(1) Tian, Y.; Xu, B.; Yu, D.; Ma, Y.; Wang, Y.; Jiang, Y.; Hu, W.; Tang, C.; Gao, Y.; Luo, K.; Zhao, Z.; Wang, L.-M.; Wen, B.; He, J.; Liu, Z. *Nature* **2013**, *493*, 385.

(2) Kern, G.; Kresse, G.; Hafner, J. *Phys. Rev. B* **1999**, *59*, 8551.

(3) Miyata, N.; Moriki, K.; Mishima, O.; Fujisawa, M.; Hattori, T. *Phys. Rev. B* **1989**, *40*, 12028.

(4) Xu, Y.-N.; Ching, W. Y. *Phys. Rev. B* **1991**, *44*, 7787.

(5) Christensen, N. E.; Gorczyca, I. *Phys. Rev. B* **1994**, *50*, 4397.

(6) Li, X.; Zhao, J.; Yang, J. *Sci. Rep.* **2013**, *3*, 1858, DOI: 10.1038/srep01858 (accessed May 17, 2013).

(7) Häussermann, U.; Simak, S. I.; Ahuja, R.; Johansson, B. *Phys. Rev. Lett.* **2003**, *90*, 065701.

(8) Sun, J.; Martinez-Canales, M.; Klug, D. D.; Pickard, C. J.; Needs, R. J. *Phys. Rev. Lett.* **2013**, *111*, 175502.

(9) Hromadová, L.; Martoňák, R. *Phys. Rev. B* **2011**, *84*, 224108.

(10) Wen, B.; Zhao, J.; Melnik, R.; Tian, Y. *Phys. Chem. Chem. Phys.* **2011**, *13*, 14566.

(11) He, C.; Sun, L.; Zhang, C.; Peng, X.; Zhang, K.; Zhong, J. *Phys. Chem. Chem. Phys.* **2012**, *14*, 10967.

(12) Éric, G.; Gang, S.; Qing-Rong, Z. *J. Phys.: Condens. Matter* **2013**, *25*, 125504.

(13) Huang, Q.; Yu, D.; Zhao, Z.; Fu, S.; Xiong, M.; Wang, Q.; Gao, Y.; Luo, K.; He, J.; Tian, Y. *J. Appl. Phys.* **2012**, *112*, 053518.

(14) Jiang, X.; Zhao, J.; Ahuja, R. *J. Phys.: Condens. Matter* **2013**, *25*, 122204.

(15) Zeng, H.; Zhi, C.; Zhang, Z.; Wei, X.; Wang, X.; Guo, W.; Bando, Y.; Golberg, D. *Nano Lett.* **2010**, *10*, 5049.

(16) Enyashin, A. N.; Ivanovskii, A. L. *Chem. Phys. Lett.* **2011**, *509*, 143.

(17) Blase, X.; Rubio, A.; Louie, S. G.; Cohen, M. L. *Europhys. Lett.* **1994**, *28*, 335.

(18) Rubio, A.; Corkill, J. L.; Cohen, M. L. *Phys. Rev. B* **1994**, *49*, 5081.

(19) Xiang, H. J.; Yang, J.; Hou, J. G.; Zhu, Q. *Phys. Rev. B* **2003**, *68*, 035427.

(20) Park, C.-H.; Louie, S. G. *Nano Lett.* **2008**, *8*, 2200.

(21) Zhang, Z.; Guo, W. *Phys. Rev. B* **2008**, *77*, 075403.

(22) Zhou, S. Y.; Gweon, G. H.; Fedorov, A. V.; First, P. N.; de Heer, W. A.; Lee, D. H.; Guinea, F.; Castro Neto, A. H.; Lanzara, A. *Nat. Mater.* **2007**, *6*, 770.

(23) Xiang, H. J.; Huang, B.; Kan, E.; Wei, S.-H.; Gong, X. G. *Phys. Rev. Lett.* **2013**, *110*, 118702.

(24) Botti, S.; Flores-Livas, J. A.; Amsler, M.; Goedecker, S.; Marques, M. A. L. *Phys. Rev. B* **2012**, *86*, 121204.

(25) Tahini, H.; Chroneos, A.; Grimes, R. W.; Schwingenschlögl, U.; Dimoulas, A. *J. Phys.: Condens. Matter* **2012**, *24*, 195802.

(26) Zhang, Z.; Guo, W. *Nano Lett.* **2012**, *12*, 3650.

(27) Wang, Y.; Ding, Y.; Ni, J. *Phys. Rev. B* **2010**, *81*, 193407.

(28) Lopez-Bezanilla, A.; Huang, J.; Terrones, H.; Sumpter, B. G. *Nano Lett.* **2011**, *11*, 3267.

(29) Kresse, G.; Furthmüller, J. *Phys. Rev. B* **1996**, *54*, 11169.

(30) Blöchl, P. E. *Phys. Rev. B* **1994**, *50*, 17953.

(31) Perdew, J. P.; Burke, K.; Ernzerhof, M. *Phys. Rev. Lett.* **1996**, *77*, 3865.

(32) Perdew, J. P.; Ruzsinszky, A.; Csonka, G. I.; Vydrov, O. A.; Scuseria, G. E.; Constantin, L. A.; Zhou, X.; Burke, K. *Phys. Rev. Lett.* **2008**, *100*, 136406.

(33) Heyd, J.; Scuseria, G. E.; Ernzerhof, M. *J. Chem. Phys.* **2003**, *118*, 8207.

(34) Heyd, J.; Scuseria, G. E.; Ernzerhof, M. *J. Chem. Phys.* **2006**, *124*, 219906.

(35) Monkhorst, H. J.; Pack, J. D. *Phys. Rev. B* **1976**, *13*, 5188.

(36) Baroni, S.; de Gironcoli, S.; Dal Corso, A.; Giannozzi, P. *Rev. Mod. Phys.* **2001**, *73*, 515.

(37) Togo, A.; Oba, F.; Tanaka, I. *Phys. Rev. B* **2008**, *78*, 134106.

(38) Bader, R. F. W. *Chem. Rev.* **1991**, *91*, 893.

(39) Henkelman, G.; Arnaldsson, A.; Jónsson, H. *Comput. Mater. Sci.* **2006**, *36*, 354.

(40) Sanville, E.; Kenny, S. D.; Smith, R.; Henkelman, G. *J. Comput. Chem.* **2007**, *28* (5), 899−908.

(41) Tang, W.; Sanville, E.; Henkelman, G. *J. Phys.: Condens. Matter* **2009**, *21*, 084204.

(42) Ayala, P.; Arenal, R.; Loiseau, A.; Rubio, A.; Pichler, T. *Rev. Mod. Phys.* **2010**, *82*, 1843.

(43) Pierce, G. A.; Aldridge, S.; Jones, C.; Gans-Eichler, T.; Stasch, A.; Coombs, N. D.; Willock, D. J. *Angew. Chem., Int. Ed.* **2007**, *46*, 2043.

(44) Winkelhaus, D.; Vishnevskiy, Y. V.; Berger, R. J. F.; Stammler, H.-G.; Neumann, B.; Mitzel, N. W. *Z. Anorg. Allg. Chem.* **2013**, *639*, 2086.

(45) Strout, D. L. *J. Phys. Chem. A* **2000**, *104*, 3364.

(46) Oku, T.; Nishiwaki, A.; Narita, I.; Gonda, M. *Chem. Phys. Lett.* **2003**, *380*, 620.

(47) Becke, A. D.; Edgecombe, K. E. *J. Chem. Phys.* **1990**, *92*, 5397.

(48) Savin, A.; Jepsen, O.; Flad, J.; Andersen, O. K.; Preuss, H.; von Schnering, H. G. *Angew. Chem., Int. Ed.* **1992**, *31*, 187.

(49) Silvi, B.; Savin, A. *Nature* **1994**, *371*, 683.

(50) Sun, Q.; Wang, Q.; Yu, J. Z.; Kumar, V.; Kawazoe, Y. *Phys. Rev. B* **2001**, *63*, 193408.

(51) Tang, H.; Ismail-Beigi, S. *Phys. Rev. Lett.* **2007**, *99*, 115501.

(52) Kortus, J.; Mazin, I. I.; Belashchenko, K. D.; Antropov, V. P.; Boyer, L. L. *Phys. Rev. Lett.* **2001**, *86*, 4656.

(53) Singh, P. P. *Phys. Rev. Lett.* **2001**, *87*, 087004.

(54) Kiran, B.; Phukan, A. K.; Jemmis, E. D. *Inorg. Chem.* **2001**, *40*, 3615.

(55) Islas, R.; Chamorro, E.; Robles, J.; Heine, T.; Santos, J.; Merino, G. *Struct. Chem.* **2007**, *18*, 833.

(56) Bucknum, M. J.; Hoffmann, R. *J. Am. Chem. Soc.* **1994**, *116*, 11456.

(57) Bucknum, M. J. *Carbon* **1997**, *35*, 1.

(58) Bucknum, M.; Castro, E. *J. Math. Chem.* **2004**, *36*, 381.

(59) Eremets, M. I.; Troyan, I. A. *Nat. Mater.* **2011**, *10*, 927.

(60) Yao, Y.; Tse, J. S.; Klug, D. D. *Phys. Rev. Lett.* **2009**, *102*, 115503.

(61) Guillaume, C. L.; Gregoryanz, E.; Degtyareva, O.; McMahon, M. I.; Hanfland, M.; Evans, S.; Guthrie, M.; Sinogeikin, S. V.; Mao, H. K. *Nat. Phys.* **2011**, *7*, 211.

(62) Lv, J.; Wang, Y.; Zhu, L.; Ma, Y. *Phys. Rev. Lett.* **2011**, *106*, 015503.

(63) Ma, Y.; Eremets, M.; Oganov, A. R.; Xie, Y.; Trojan, I.; Medvedev, S.; Lyakhov, A. O.; Valle, M.; Prakapenka, V. *Nature* **2009**, *458*, 182.

(64) Wang, Z.; Okude, M.; Saito, M.; Tsukimoto, S.; Ohtomo, A.; Tsukada, M.; Kawasaki, M.; Ikuhara, Y. *Nat. Commun.* **2010**, *1*, 106.

(65) Chatterjee, S.; Kim, M. J.; Zakharov, D. N.; Kim, S. M.; Stach, E. A.; Maruyama, B.; Sneddon, L. G. *Chem. Mater.* **2012**, *24*, 2872.

(66) Kim, S.-K.; Cho, H.; Kim, M. J.; Lee, H.-J.; Park, J.-h.; Lee, Y.-B.; Kim, H. C.; Yoon, C. W.; Nam, S. W.; Kang, S. O. *J. Mater. Chem., A* **2013**, *1*, 1976.

(67) Ayme, J.-F.; Beves, J. E.; Campbell, C. J.; Leigh, D. A. *Chem. Soc. Rev.* **2013**, *42*, 1700.